Design of a Two-Body Wave Energy Converter Featuring Controllable Geometry

Preprint

Nathan Tom,[1] David Ogden,[2] and Michaela Byrne[3]

1 National Renewable Energy Laboratory
2 Velocity Global
3 Ohio University

Presented at ASME 2023 42nd International Conference on Ocean, Offshore and Arctic Engineering (OMAE 2023)
Melbourne, Australia
June 11–16, 2023

NREL is a national laboratory of the U.S. Department of Energy
Office of Energy Efficiency & Renewable Energy
Operated by the Alliance for Sustainable Energy, LLC

This report is available at no cost from the National Renewable Energy Laboratory (NREL) at www.nrel.gov/publications.

Contract No. DE-AC36-08GO28308

Conference Paper
NREL/CP-5700-85028
June 2023

Design of a Two-Body Wave Energy Converter Featuring Controllable Geometry

Preprint

Nathan Tom,[1] David Ogden,[2] and Michaela Byrne[3]

1 National Renewable Energy Laboratory
2 Velocity Global
3 Ohio University

Suggested Citation
Tom, Nathan, David Ogden, and Michaela Byrne. 2023. *Design of a Two-Body Wave Energy Converter Featuring Controllable Geometry: Preprint*. Golden, CO: National Renewable Energy Laboratory. NREL/CP-5700-85028.
https://www.nrel.gov/docs/fy23osti/85028.pdf.

NREL is a national laboratory of the U.S. Department of Energy
Office of Energy Efficiency & Renewable Energy
Operated by the Alliance for Sustainable Energy, LLC

This report is available at no cost from the National Renewable Energy Laboratory (NREL) at www.nrel.gov/publications.

Contract No. DE-AC36-08GO28308

Conference Paper
NREL/CP-5700-85028
June 2023

National Renewable Energy Laboratory
15013 Denver West Parkway
Golden, CO 80401
303-275-3000 • www.nrel.gov

NOTICE

This work was authored in part by the National Renewable Energy Laboratory, operated by Alliance for Sustainable Energy, LLC, for the U.S. Department of Energy (DOE) under Contract No. DE-AC36-08GO28308. Funding provided by U.S. Department of Energy Office of Energy Efficiency and Renewable Energy Water Power Technologies Office. The views expressed herein do not necessarily represent the views of the DOE or the U.S. Government. The U.S. Government retains and the publisher, by accepting the article for publication, acknowledges that the U.S. Government retains a nonexclusive, paid-up, irrevocable, worldwide license to publish or reproduce the published form of this work, or allow others to do so, for U.S. Government purposes.

Cover Photos by Dennis Schroeder: (clockwise, left to right) NREL 51934, NREL 45897, NREL 42160, NREL 45891, NREL 48097, NREL 46526.

DESIGN OF A TWO-BODY WAVE ENERGY CONVERTER FEATURING CONTROLLABLE GEOMETRY

Nathan Tom*
National Renewable
Energy Laboratory
Golden, CO
Email: Nathan.Tom@nrel.gov

David Ogden
Velocity Global
London, United Kingdom
Email: david.ogden.nrel@outlook.com

Michaela Byrne
Ohio University
Athens, OH
Email: mb454316@ohio.edu

ABSTRACT

While the field of wave energy has been the subject of numerical simulation, scale model testing, and precommercial project testing for decades, wave energy technologies remain in the early stages of development and must continue to prove themselves as a promising modern renewable energy field. A wave energy converter (WEC) concept currently being explored is the variable-geometry WEC (VGWEC), which aims to add an extra control option to WEC design. VGWECs attempt to incorporate controllable geometric features to adjust the floating body hydrodynamics to favor either power absorption, load shedding, or other operational goals. These variable geometry components have been proposed to be controlled on a sea-state-to-sea-state or wave-to-wave time scale depending on the force (or torque) and bandwidth limitations of the actuators required to manipulate just the controllable geometric hull features. Having control over both the WEC geometry components and the power take-off (PTO) offers the potential to improve overall system performance and reliability if a cost-effective solution can be found for a given WEC architecture. This paper will present the recent developments and results of a VGWEC concept that incorporates variable-geometry modules into a two-body WEC. In the proposed VGWEC concept, the variable-geometry modules consist of air-inflatable bags in the surface float and a water inflatable ring in the subsurface body. The surface float is tethered directly to the subsurface body through tether lines, each connected to a separate PTO. Adjusting the geometry of both the surface and subsurface bodies along with the PTO coefficients can maximize power in design sea states while reducing motion response and PTO forces when transitioning to sea states where rated power is reached and load shedding is prioritized. The ability to transition between operating condition is expected to increase the sea state operational map and power capacity.

1 INTRODUCTION

The National Renewable Energy Laboratory (NREL) has continued its investigation into the load shedding capabilities of variable-geometry wave energy converters (VGWECs) since its initial publication in 2016 on a variable-geometry oscillating surge wave energy converter [1]. The emphasis of VGWECs is to add a hydrodynamic control knob on top of power take-off (PTO) control to improve performance and reduce structural loading [2]. NREL considers a VGWEC to be any device that can actively or passively control WEC hydrodynamics. While actively controlled actuated surfaces are one approach, hydrodynamics can also be controlled by changing the submergence depth with seawater ballasting (or another method). Regardless of desired implementation, the ability to control the device hydrodynamics allows for greater load shedding capabilities to improve WEC survivability. The expectation is that any WEC will have a PTO with rated power and force that will limit WEC control in larger seas. Rather than attempt to overdesign the PTO, the variable-geometry components can be adjusted to shed loads and maintain rated power over a wider set of operating condi-

*Address all correspondence to this author.

tions, as proposed in Fig. 1.

VGWECs are relatively new to the wave energy industry, but there are several examples of developers that are applying the same concepts within their own technologies. For example, large-scale geometric changes are included in the WEPTOS design [3], which is initially deployed in an "A" frame pointing into the waves. As the wave climate increases, a controllable cross beam will move toward the back of the WEC, causing the frontal area of the device to become narrower, which lets more wave power pass through. California-based CalWave [4] is actively developing their xWave technology, which is a single submerged body that is connected directly to the seabed via four PTO tethers. The xWave technology is able to control hydrodynamics through a controllable central opening that creates a wave pressure pass-through. It can also wind up the four tether lines to increase the submergence depth to avoid storm conditions. Another example is the Monterey Bay Aquarium Research Institute's WEC, which is a two-body point absorber with a conical heave plate that is divided into six pieces [5]. Three of the pieces are connected to a yaw actuator that is activated in larger sea states to rotate and create openings in the conical heave plate to reduce hydrodynamic pressure. These three WEC technologies are a small subset of the larger WEC community but demonstrate that some developers have decided that incorporating controllable geometry is key to their operation.

This study is a continuation of previous research performed on a variable-geometry two-body wave energy converter [6]. The proposed variable-geometry two-body WEC incorporates controllable geometric features using inflatables in both the surface and subsurface bodies that allow the WEC to transition from an inflated (power maximization) to deflated (load shedding) state. The use of inflatables integrated into the WEC structure has been previously explored in attenuator WECs [7,8], and the Wave Energy Scotland Net Buoy project hopes to reduce material costs by designing inflatable structures as the prime movers. Furthermore, other prior investigations have considered coupling the breathing-like action of air-filled bags to harness wave energy [9]. The use of inflatable features is attractive because flexible fabrics are anticipated to be less expensive than steel, and deflation upon deployment and recovery should decrease costs associated with operation and maintenance.

This paper extends the numerical model development first introduced in [6] by focusing on the performance differences between the inflated and deflated states. Ogden et al. [6] focused on exploring the initial design space and estimating the preliminary costs by calculating the ACE metric, derived as part of the U.S. Department of Energy Wave Energy Prize [10], which is a simplified ratio of power produced over the cost of structural materials to build the wave activated bodies to be a proxy for levelized cost of energy. This paper begins with an introduction to the details of the two-body VGWEC concept and the proposed method of operation. Then, greater detail is focused on the geometric and mass properties modeling, which assists in describing how much influence controllable geometries have relative to static geometries. Next, an analysis is presented of the efforts required to maintain hydrostatic equilibrium for a two-body system with asymmetric mass properties and tether connections, illustrating how the tether pretensions also need to be controllable to allow for the shape change. Finally, results from dynamic simulations of a scaled-down version of the two-body VGWEC are presented to compare performance between the inflated and deflated configurations.

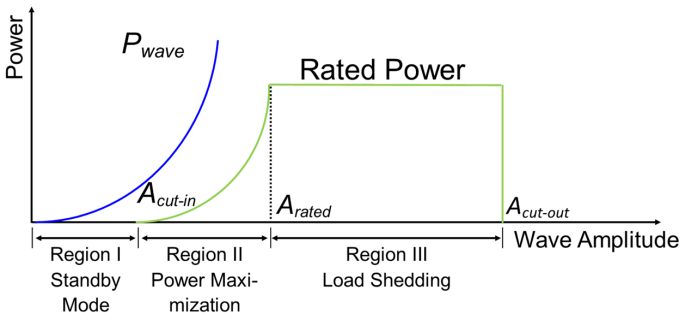

FIGURE 1. PROPOSED WEC POWER CURVE INDICATING TRANSITION FROM MAXIMIZING POWER CAPTURE TO MAINTAINING RATED POWER.

2 DESCRIPTION OF THE TWO-BODY VGWEC

One promising design that has emerged from a recent exploratory study into different VGWECs [6,8,11] is the two-body WEC that incorporates controllable geometric features using inflatables that allow the WEC to transition from an inflated to a deflated state, as shown in Fig. 2. The VGWEC transitions from the inflated to deflated state in larger wave environments to emphasize power maximization over load shedding. In the proposed variable-geometry design, the surface-piercing body comprises a steel structural core (the green portion in Fig. 2) with side airbags that are filled with air (the blue portions in Fig. 2). The surface body is connected to the subsurface body through three tether lines—two fore and one aft—which is similar to Oscilla Power's Triton WEC [12]. The subsurface body comprises a central concrete disk, which provides the structural strength to withstand the tether tension (the gray portion in Fig. 2), and the disk is surrounded by a water-filled inflatable torus (the red portion in Fig. 2). The inflatables were chosen, as a simplified analysis of the levelized cost of energy showed that using solely steel for the entire geometry would quickly drive up costs, whereas the desired shape could be augmented with flexible coated fabrics that

could be inflated with the air and water found at the deployment location. A key assumption is that the cost of coated fabrics and pumps would be less than the cost of steel. The following sections will describe the modeling approach used to simulate the response of this two-body VGWEC; however, a significant assumption is that a feasible inflatable structure could be designed to maintain the idealized shapes.

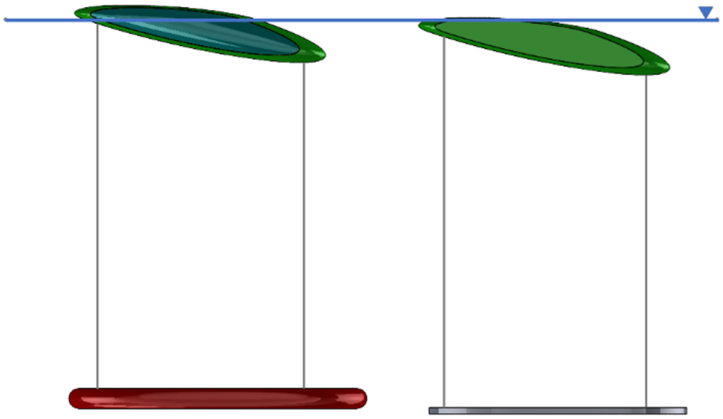

(a) SIDE VIEW

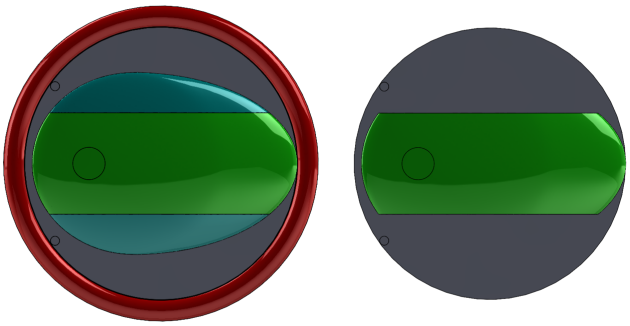

(b) TOP-DOWN VIEW

FIGURE 2. SOLIDWORKS RENDERING OF THE TWO-BODY POINT ABSORBER WITH VARIABLE GEOMETRY. (LEFT) INFLATED WEC STATE FOR POWER MAXIMIZATION AND (RIGHT) DEFLATED WEC STATE FOR LOAD SHEDDING. THE BLUE SIDE PIECES IN THE SURFACE FLOAT ARE AIR INFLATABLES, AND THE RED TOROIDAL PIECE IN THE SUBSURFACE FLOAT IS A WATER INFLATABLE. IN THE DEFLATED STATE THE LOSS OF BUOYANCY CAUSES THE WEC TO SIT DEEPER IN THE WATER COLUMN. IN THIS IMAGE THE WAVES WILL COME FROM LEFT TO RIGHT; THUS, THE FORE OF THE WEC IS PROTRUDING OUT OF THE WATER.

FIGURE 3. (LEFT) SOLIDWORKS CAD MODEL OF A HEMISPHERE WITH A RADIUS OF 10 M AS DESCRIBED BY EQN. (1) AND (RIGHT) CAD MODEL OF THE 10 M RADIUS HEMISPHERE WITH X_{SHEAR} OF 1.5 AND Z_{SCALE} OF 0.5 APPLIED AS DESCRIBED BY EQNS. (3) AND (4)

2.1 Design of the Surface Body

The initial concept for the two-body floating point absorber initially featured a sphere floating at the water surface connected to a submerged reaction body via four tethers. But [13] demonstrated how the performance of a floating hemisphere can be improved by applying a combination of shear mapping (in the x-direction) and scaling (in the z-direction) to generate an ellipsoid geometry similar to the Edinburgh Duck [14]. To understand the generation of the ellipsoid geometry, we begin with the implicit equation of a sphere, which is given by:

$$x_h^2 + y_h^2 + z_h^2 = R_h^2 \tag{1}$$

where R is the radius of the sphere. Since any horizontal cuts through the x-y plane will generate circles, one can determine the radius of these circular cuts from the following simplified expression:

$$x_h^2 + z_h^2 = R_h^2 \tag{2}$$

where, here, x is equivalent to the circular cross-section radius. These surface expressions for the hemisphere were calculated before applying the x-shear mapping and the z-scaling. These mapping and scaling transformations were completed as follows:

$$x_{sh} = x_h + x_{shear} z_h \tag{3}$$

$$z_{sh} = z_{scale} z_h \tag{4}$$

2.2 Design of the Subsurface Body

The core of the subsurface body is a solid disk (assumed to be concrete) with a torus connected to the outside edge of the disc (Fig. 4), which is made from a coated fabric and filled with water. To achieve hydrostatic equilibrium with the surface body, the requirements are that (1) the subsurface body has a net weight

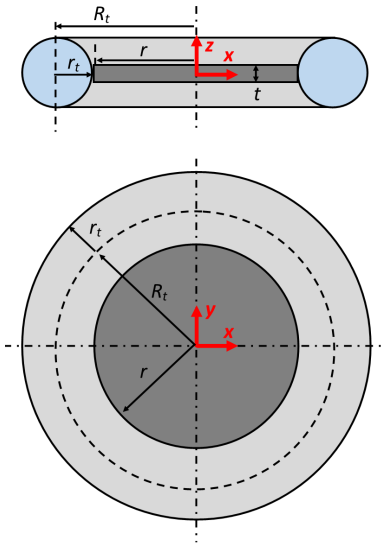

FIGURE 4. (TOP) SIDE AND (BOTTOM) TOP-DOWN SCHEMATIC DEFINING THE MAJOR AND MINOR RADIAL DIMENSIONS NEEDED TO DEFINE THE MASS PROPERTIES OF THE CENTRAL DISK AND OUTER TOROID. THE DARK GRAY SECTION DENOTES THE INNER CONCRETE DISK, THE LIGHT GRAY SECTION DENOTES THE FLEXIBLE COATED FABRIC, AND THE LIGHT BLUE SECTIONS DENOTE ENTRAPPED SEA WATER.

equivalent to the net buoyancy of the surface body and (2) the size of the solid disk has to be sufficient to allow the tether attachment points to align with the surface body, resulting in the moments on the reaction body canceling out. These requirements restrict the number of geometric parameters that could be explored for optimizing the subsurface body. More information can be found in [6].

2.2.1 Modeling Inertial Properties of the Subsurface Body Starting with the central solid disk reaction body, shown as dark gray in Fig. 4, the mass properties can be calculated from the following expression:

$$\forall_d = \pi r^2 t \tag{5}$$

$$m_d = \rho_d \pi r^2 t \tag{6}$$

$$I_{d,44} = I_{d,55} = \frac{m_d r^2}{4}\left[1+\frac{1}{3}\left(\frac{t}{r}\right)^2\right] = \frac{\rho_d \pi r^4 t}{4}\left[1+\frac{1}{3}\left(\frac{t}{r}\right)^2\right] \tag{7}$$

$$\underbrace{\approx}_{\frac{t}{r}\ll 1} \frac{\rho_d \pi r^4 t}{4} \tag{8}$$

where V_d is the disk displaced volume, r is the radius of the disk, t is the thickness of the disk, m_d is the mass of the disk, ρ_d is the material density of the disk, $I_{d,44}$ is the disk mass moment of inertia in roll, and $I_{d,55}$ is the disk mass moment of inertia in pitch. Under the assumption that the material density is uniform, it is not unexpected that the radius of the solid disk will be the dominant parameter when estimating mass and moment of inertia.

The geometric shape of the toroidal ring, shown as light gray in Fig. 4, can be defined by the major radius, R_t, and minor radius, r_t, which allow for toroidal mass properties to be calculated as follows:

$$\forall_t = 2\pi^2 R_t r_t^2 \tag{9}$$

$$m_t = \rho_t 2\pi^2 R_t r_t^2 \tag{10}$$

$$I_{t,44} = I_{t,55} = \frac{m_t}{8}\left(4R_t^2+5r_t^2\right) = \rho_t \pi^2 r_t^2 R_t^3\left[1+\frac{5}{4}\left(\frac{r_t}{R_t}\right)^2\right] \tag{11}$$

$$\underbrace{\approx}_{\frac{r_t}{R_t}\ll 1} \rho_t \pi^2 r_t^2 R_t^3 = \rho_t \pi^2 r^3 r_t^2\left(1+\frac{r_t}{r}\right)^3 \tag{12}$$

where V_t is the toroidal displaced volume, m_t is the mass of the disk, ρ_t is the material density of the toroid, $I_{t,44}$ is the toroid mass moment of inertia in roll, and $I_{t,55}$ is the toroid mass moment of inertia in pitch. In the presented design, the mass of the coated fabric is assumed negligible compared to the mass of the entrapped water. As a result, the toroidal density can be replaced with the density of water. One can observe from Eqn. (10) that the mass of entrapped water is proportional to the square of the toroid radius while the radius of the internal disk is fixed. The moment of inertia is also proportional to the square of the toroid radius, but a larger contribution is to the cube of the internal disk radius. From these expressions we can expect that the entrapped water is going to increase the total moment of inertia of the reaction body more than it increases the total mass.

2.2.2 Toroidal Surface Area As previously discussed in [6], the cost of the reaction body is related to the surface area of the toroid (assuming the cost of the fabric is reported in \$/m^2). Therefore, expressing the surface area of the toroid as a function of the same geometric parameters used to estimate the mass properties would shed light on how much more the design might cost if it is desired to use a larger toroid to capture more of the surrounding water. The expression for the surface area of a toroid using the same variables described in the previous sections is

given by the following:

$$SA_t = 2\pi t_r \left[2\pi \left(r + t_r\right)\right] = 4\pi^2 t_r r \left(1 + \frac{t_r}{r}\right) \underbrace{\approx}_{\frac{t_r}{r} \ll 1} 4\pi^2 t_r r \quad (13)$$

Thus, for small $\frac{t_r}{t}$, the surface area of the toroid increases linearly with the toroid radius. Therefore, as the toroid radius is increased in an attempt to entrap a greater amount of water, the resulting increase in power capture also needs to be linear to have a near constant cost of energy estimate.

3 HYDROSTATIC EQUILIBRIUM CALCULATIONS

The surface and subsurface floats are connected via nonsymmetric tethers, and the tension in each tether will need to be calculated to ensure hydrostatic equilibrium. In order to calculate the required tensions, the following system of equations was established that allows the tensions to be adapted as different WEC properties are iterated:

$$\begin{aligned} f_{W,1} &= m_1 g \ , \ f_{B,1} = \rho \forall_1 g && (14)\\ f_{h,1} &= f_{B,1} - f_{W,1} = \left(\rho \forall_1 - m_1\right) g \\ \sum F_{z,1} &= 0 = 2T_f + T_a + f_{h,1} && (15)\\ &\rightarrow 2T_f + T_a = -f_{h,1} && (16)\\ \sum M_{cg,1} &= 0 = 2T_f x_{f,1} + T_a x_{a,1} + f_{B,1} x_{cb,1} \\ &\rightarrow 2T_f x_{f,1} + T_a x_{a,1} = -f_{B,1} x_{cb,1} && (17) \end{aligned}$$

where $f_{W,1}$ is the material weight of the surface float, m_1 is the material mass of the surface float, g is gravitational acceleration, $f_{B,1}$ is the buoyancy force of the surface float, ρ is the fluid density, $\forall_1$ is the displaced volume of the surface float, $f_{h,1}$ is the net hydrostatic force of the surface float (which needs to be greater than 0), $F_{z,1}$ is the summation of forces in the vertical direction for the surface float, T_f is the fore tether tension, T_a is the aft tether tension, $M_{cg,1}$ is the summation of moments about the center of gravity of the surface float, $x_{f,1}$ is the horizontal distance from the center of gravity to the fore tether connection point, $x_{a,1}$ is the horizontal distance from the center of gravity to the aft tether connection point, and $x_{cb,1}$ is the horizontal distance from the center of gravity to the center of buoyancy of the surface float.

Equations (16) and (17) have two unknowns, T_f and T_a, assuming that the tether connection locations have already been selected and the mass properties of the body are known. This system of equations can be constructed in the traditional $Ax = B$ format as follows:

$$\begin{bmatrix} 2 & 1 \\ 2x_{f,1} & x_{a,1} \end{bmatrix} \begin{bmatrix} T_f \\ T_a \end{bmatrix} = \begin{bmatrix} -f_{h,1} \\ -f_{B,1} x_{cb,1} \end{bmatrix} \quad (18)$$

which can be solved by any linear solver. The subsurface float will require the same force and moment balance about its own center of gravity, which can be described by the following expressions:

$$\begin{aligned} f_{W,2} &= m_2 g \ , \ f_{B,2} = \rho \forall_2 g && (19)\\ f_{h,2} &= f_{B,2} - f_{W,2} = \left(\rho \forall_2 - m_2\right) g \\ \sum F_{z,2} &= 0 = 2T_f + T_a + f_{h,2} && (20)\\ &\rightarrow 2T_f + T_a = -f_{h,2} && (21)\\ \sum M_{cg,2} &= 0 = 2T_f x_{f,2} + T_a x_{a,2} + f_{B,2} x_{cb,2} \\ &\rightarrow 2T_f x_{f,2} + T_a x_{a,2} = -f_{B,2} x_{cb,2} && (22) \end{aligned}$$

where $\sum F_{z,1} + \sum F_{z,2} = 0$, which can be simplified to $f_{h,1} + f_{h,2} = 0$. The subscript 2 denotes the subsurface body while all other variables are as defined in the expressions derived for the surface float. Unlike Eqn. (18), where the unknowns are the force and aft tether tensions, the unknowns needed to maintain static equilibrium for the subsurface body are the tether connections. The additional equality constraint required to maintain a zero net moment on the surface body is that the separation distance between the fore and aft connection points on the subsurface body must be equal to the separation distance on the surface body, as shown by the following:

$$x_{f,1} - x_{a,1} = x_{f,2} - x_{a,2} \quad (23)$$

Now, Eqns. (22) and (23) can be used to set up a system of equations to solve for the two unknowns, $x_{f,2}$ and $x_{a,2}$, as follows:

$$\begin{bmatrix} 1 & -1 \\ 2T_f & T_a \end{bmatrix} \begin{bmatrix} x_{f,2} \\ x_{a,2} \end{bmatrix} = \begin{bmatrix} x_{f,1} - x_{a,1} \\ -f_{B,2} x_{cb,2} \end{bmatrix} \quad (24)$$

If the quantity $-f_{B,1} x_{cb,1} = -f_{B,2} x_{cb,2}$, then the tether connection points will be the same distance from the center of gravity for the surface and subsurface bodies, which implies the two bodies will have a center of gravity x-coordinate that will be the same; however, if the equality does not hold, then the x-coordinate of the center of gravity between the surface and subsurface bodies will be offset.

4 MASS PROPERTIES OF THE VGWEC CONFIGURATIONS

The surface and subsurface bodies were built in SolidWorks to estimate the mass and mass moment of inertia for the inflated and deflated VGWEC configurations using the material densities listed in Table 1. Comparisons of the mass properties between the VGWEC configurations are shown in Tables 2 and 3.

One can observe that between the two configurations, the total volume of the surface body is reduced by nearly 350 m^3, corresponding to the loss of the sides of the surface body (refer to Fig. 2b), whereas the displaced volume stays nearly constant as a result of the unchanging net weight in the subsurface body. In the tables, the material masses of the toroid and entrapped water are included for the subsurface body; however, these contributions are neutrally buoyant. As a consequence of the lost volume on the sides of the surface body, the draft is increased and the surface body sits lower in the water (refer to Fig. 2a). In addition, this change in displaced volume also causes the center of buoyancy to move forward as more of the displaced volume moves forward as a result of the inclined geometry. Therefore, for each configuration, the pretension forces in the fore and aft PTOs need to be updated to maintain the desired trim. Yet if the shift in the center of buoyancy is too great while assuming a static center of gravity, there may not be a feasible solution to Eqn. (24), as a greater distance between the PTO connection points and the center of gravity of the subsurface body is needed while the distance of the PTO connection points on the surface body are assumed fixed. There is the potential to slightly angle the tethers as they move from the surface to the subsurface body; a slight angle of 1–2 degrees will have minimal effect on the net tension and, with a separation distance of 44 m, can lead to sufficient distance in the x-direction to achieve the needed moment balance.

TABLE 1. Density of Materials Found in the VGWEC Structure

Material	Density	Units
Steel	7850	kg m^{-3}
Concrete	2450	kg m^{-3}
Water	1000	kg m^{-3}
Air	1.22	kg m^{-3}

5 HYDRODYNAMIC MODELING AND SIMULATION

Both configurations of the VGWEC were built in SolidWorks, providing the mass, volume, and mass moments of inertia at full scale. In preparation for wave tank tests that were completed earlier in 2023 at the Stevens Institute of Technology in Hoboken, New Jersey, the CAD models and mass properties were then scaled by a 1:35 ratio to match the dimensions of the wave tank. The three-dimensional models were then meshed in Rhinoceros [15], a separate modeling software, for use in the hydrodynamic modeling tool WAMIT [16].

Both the inflated and deflated configurations were simulated using WEC-Sim [17], an open-source tool developed by NREL and Sandia National Laboratories. Using hydrodynamic coefficients obtained from WAMIT, WEC-Sim is able to simulate the response of a variety of wave energy converters in various sea states. WEC-Sim was used to measure the VGWEC power production, PTO extension, and displacements of both bodies. In order to compare the variable performance of the VGWEC, a

TABLE 2. Mass Properties for the Inflated VGWEC

Variable	Surface Body	Subsurface Body	Units
Material Mass	269,549	1,735,782	kg
Center of Gravity	[6.0, 0.0 ,−2.0]	[5.5,0.0,−44.0]	m
Center of Buoyancy	[5.6,0.0,−1.9]	[5.4,0.0,−44.0]	m
Roll Moment of Inertia	3,375,447	130,616,894	kg m^2
Pitch Moment of Inertia	14,281,342	130,616,894	kg m^2
Yaw Moment of Inertia	16,025,636	260,812,965	kg m^2
Displaced Volume	1047	967	m^3
Total Volume	1396	967	m^3

TABLE 3. Mass Properties for the Deflated VGWEC

Variable	Surface Body	Subsurface Body	Units
Material Mass	269,121	1,298,852	kg
Center of Gravity	[6.0,0.0, −3.4]	[3.4,0.00,−45.4]	m
Center of Buoyancy	[4.1,0.0,−2.8]	[3.4,0.0,−45.4]	m
Roll Moment of Inertia	3,352,237	73,121,320	kg m^2
Pitch Moment of Inertia	14,265,566	73,121,320	kg m^2
Yaw Moment of Inertia	15,987,756	146,120,873	kg m^2
Displaced Volume	1037	530	m^3
Total Volume	1047	530	m^3

regular wave sweep was conducted where the wave period was varied while the wave height was held constant, with all waves coming head-on (0 degree wave heading) and simulations run for 4 minutes (a detailed list of wave conditions can be found in Table 4).

TABLE 4. WAVE CONDITIONS FOR REGULAR WAVE SWEEP.

Case	Period, T [s]	Height, H [m]	Heading, θ [deg]
A	0.75	0.01	0
B	1.00	0.01	0
C	1.25	0.01	0
D	1.50	0.01	0
E	1.75	0.01	0
F	2.00	0.01	0
G	2.25	0.01	0
H	2.50	0.01	0
I	2.75	0.01	0
J	3.00	0.01	0

6 RESULTS OF REGULAR WAVE SWEEP

The performance metrics measured from WEC-Sim simulations are presented in the following sections to illustrate the difference in response between the inflated and deflated configurations.

6.1 Surface and Subsurface Body Displacement

As shown in Fig. 5, the surface body had significantly larger translational motion compared to the subsurface body while having similar rotational displacement. This is not unexpected, as the design of the two-body system emphasizes excitation of the surface float while designing the subsurface body to provide a large reaction force to maximize relative motion for improved power capture. A slightly unexpected result was how surge exceeded heave displacement by a significant factor, especially between 0.5 and 0.8 Hz. Upon reflection, this is likely a result of tether lines oriented completely vertical, as the pretension forces lead to minimal restoring stiffness and damping, and with perhaps lower surge wave damping leading to larger amplitudes of motion. A more interesting result is the observation of the difference between the inflated and deflated cases for pitch motion at lower frequencies. The inflated configuration has the largest pitch motion at the longest waves simulated, whereas the deflated configuration has nearly no rotational motion as well as minimal surge and heave motion. Such a response was desired because it allows the WEC to become invisible to the waves, especially at longer waves expected with storm conditions. The reason for the increased pitch response at the longer wave periods is likely from the heave-pitch coupling that results from the asymmetric profile of the surface body. As shown in Fig. 2b, a larger portion of the geometry sits in front of the center of gravity, which results in pitch motion when the surface float moves up and down. When transitioning to the deflated configuration, the bulk of the geometry remains more central, reducing the impact of any heave-pitch coupling. For the subsurface body a similar reduction in general motion is observed between the inflated and deflated cases, with pitch motion showing the greatest differences.

6.2 PTO Tether Length

As shown in [11], the amplitude and phase of the 3 degrees of freedom motion of the surface float can have a large influence on the extension of the fore (PTO 1 and PTO 2) and aft (PTO 3) tether lines. From Fig. 6, one can observe that for the inflated configuration there is a transition near 0.45 Hz where the PTO tether extension is nearly the same for both fore and aft PTOs, but at lower and higher frequencies the fore and aft PTOs begin to dominate, respectively, eventually leading to greater contributions in power production. For the deflated configuration this transition is not present, and the aft PTO tether extension is much larger than that of the fore PTOs across the majority of the wave frequencies. Similar to the discussion on surface and subsurface float motion, we are encouraged to see, for longer waves, that there is minimal PTO displacement, as this should allow the WEC to be detuned at longer waves in hopes of reducing the forcing on the PTOs.

6.3 Time-Averaged Power Absorbed by PTOs

For all simulations, the same linear spring and damping coefficients were used as the PTO feedback loop to generate the power capture of the two-body system. One can thus expect that the individual and total power production follow a similar trend to the PTO extension, which is confirmed in Fig. 7. For both inflated and deflated cases, PTO 1 and PTO 2 are shown to generate the same amount of power, which is consistent with the simulation approach, as all waves came from 0 heading and no oblique wave cases were considered. From Fig. 7a it can be observed that PTO 3 has a power capacity requirement that is nearly three times that of PTO 1 and PTO 3, although this is for a very narrow banded period. This is a consequence of both the WEC design and having a fairly simple PTO feedback loop, as a more advanced PTO controller could be utilized to limit such an exceptionally large peak. When comparing the total mechanical time-averaged power absorbed by both configurations (Fig. 8)

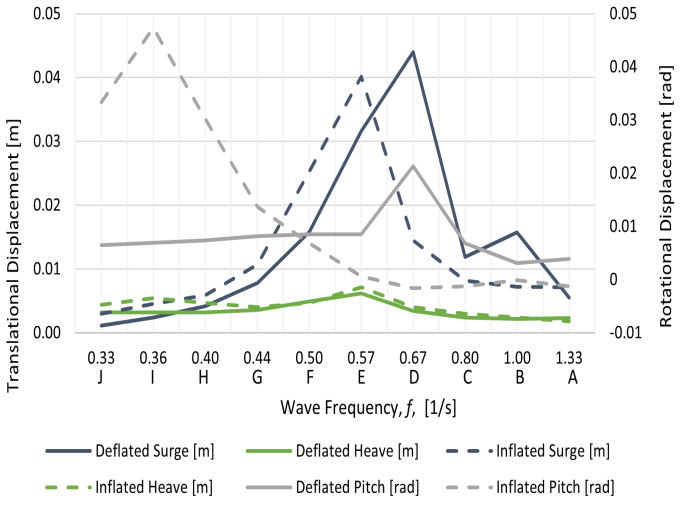

(a) SURFACE BODY

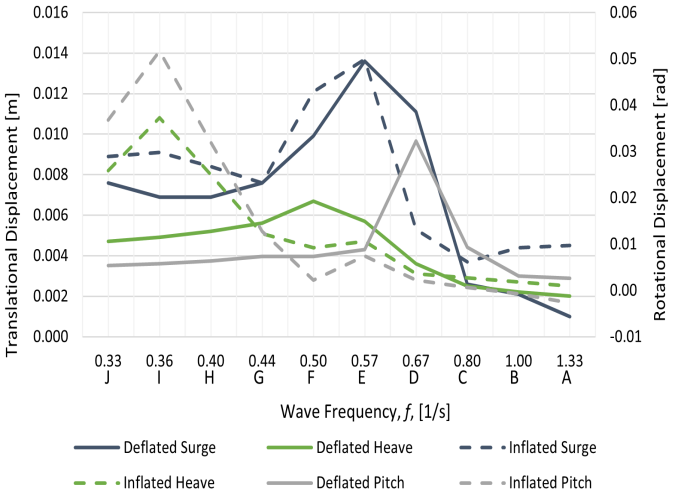

(b) SUBSURFACE BODY

FIGURE 5. COMPARISON OF MAX SURGE, HEAVE, AND PITCH DISPLACEMENT FOR THE DEFLATED AND INFLATED CONFIGURATIONS

over the entire frequency range, the inflated configuration does have a greater average absorbed power. The peak power capture for both the inflated and deflated configurations is nearly the same, although there is a shift of 0.1 Hz between peaks. A slightly unexpected result was to see the deflated case producing more power than the inflated case; granted, the overperforming range is rather small, but the designers would still have expected that with a larger geometry present, more wave forcing would have been transferred to the tethers. However, given that this peak seems to be associated with a corresponding peak in surge motion (refer to Fig. 5a), perhaps there is a surge resonance being excited that is minimally impacted by the loss of the

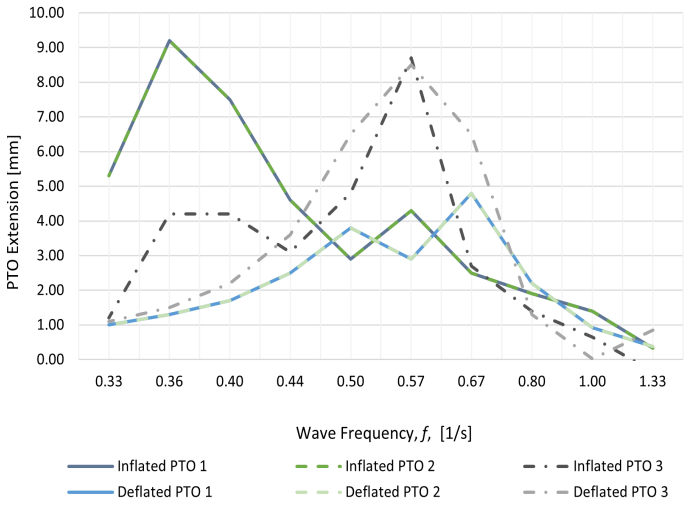

FIGURE 6. COMPARISON OF MAX PTO TETHER LENGTH EXTENSIONS BETWEEN THE INFLATED AND DEFLATED CONFIGURATIONS

inflatable side bags. In addition to the local peak in power absorption near 0.60 Hz, for the inflated case there is a local peak near 0.38 Hz that, although not as large, is still close to 60%–70% of the largest peak and would likely play a substantial role in annual energy production. The dip in performance near 0.45 Hz is somewhat undesirable, as the design team had hoped to maintain higher energy capture over a wider range of frequencies. Still, as no optimization was completed with regards to the linear spring and damping PTO coefficients, the dip may not be as pronounced with further work. Lastly, to better relate power generation to the size of the modeled WEC, the nondimensional capture width is plotted in Fig. 8b. Since the associated wave power decreases with increasing wave frequency, one can expect to see lower capture efficiencies at longer waves with efficiency peaks at higher frequencies. Although theoretically possible for a multi-degree-of-freedom resonator to capture more power than is hitting the frontal area, this comes with caveats on unmodeled dissipation mechanisms and assumptions in modeling approach. The first assumption is that the side inflatable bags retain their shape despite the more likely scenario that the bags would begin to deform at larger velocities and accelerations, resulting in additional load shedding, which should lower peak power capture. Second, with any large displacement there are going to be nonlinear viscous losses that will also reduce peak motion, which also decreases power capture [18]. As a result, the peak capture width near 0.60 Hz is likely an overestimation, but a peak efficiency closer to 50% might be achievable.

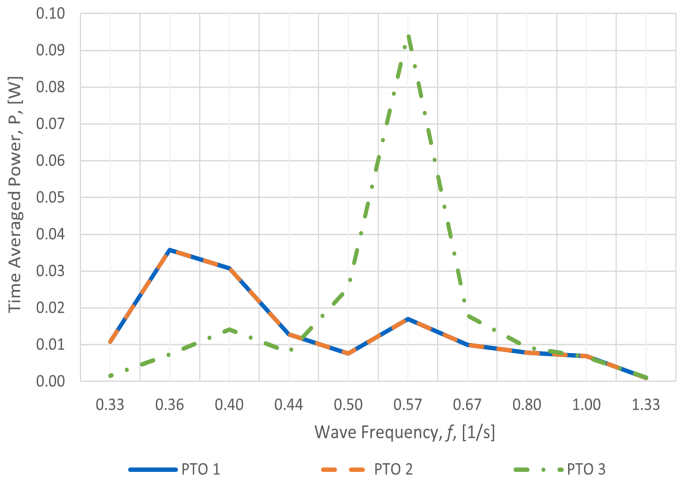

(a) INFLATED CONFIGURATION

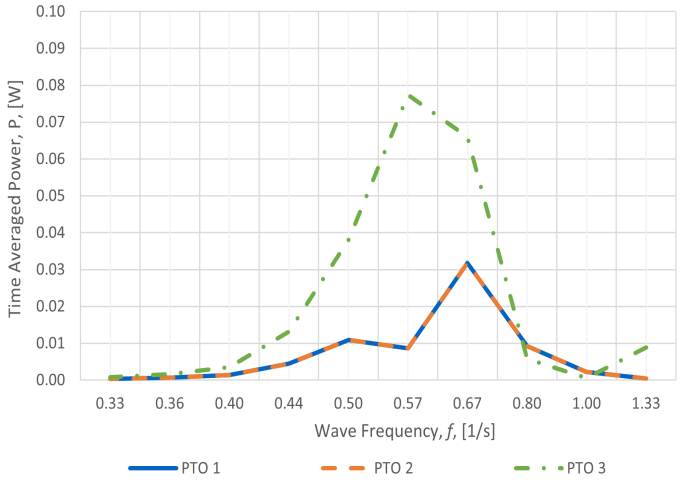

(b) DEFLATED CONFIGURATION

FIGURE 7. COMPARISON OF THE TIME-AVERAGED POWER ABSORBED BY EACH PTO AND BETWEEN THE INFLATED AND DEFLATED CONFIGURATIONS

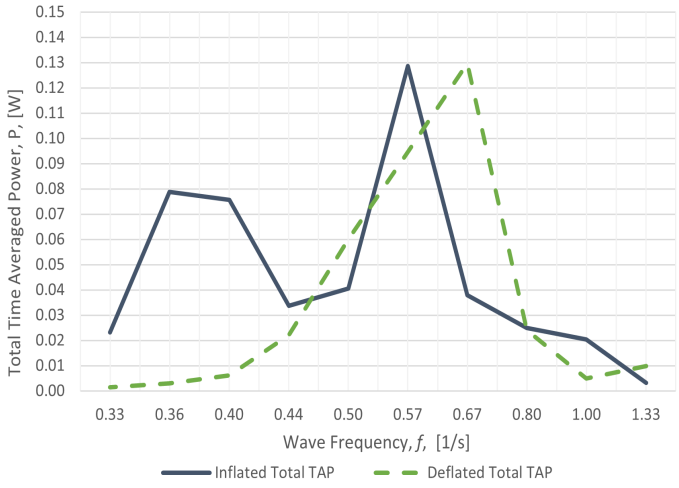

(a) TOTAL TIME AVERAGED POWER

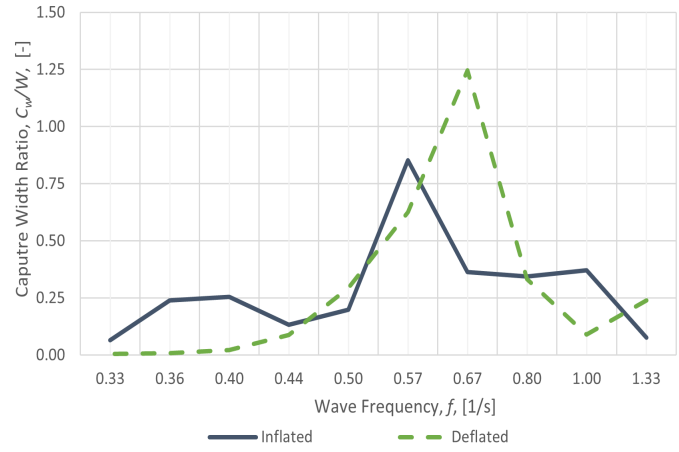

(b) NONDIMENSIONAL CAPTURE WIDTH

FIGURE 8. COMPARISON OF THE TOTAL TIME-AVERAGED POWER AND CAPTURE WIDTH RATIO BETWEEN THE INFLATED AND DEFLATED CONFIGURATIONS

7 CONCLUSIONS

The original design of the two-body VGWEC [6] has gone through additional updates and analysis, which have been highlighted in this work. The results from WEC-Sim are promising and support many of the original design objectives; however, there were unexpected responses in the deflated case that warrant further investigation to understand why equivalent max power absorption to the inflated case is being achieved. Still, the near elimination of displacement and power at long waves is expected to help the WEC ride out the largest storms and potentially extract greater power with longer waves at moderate wave heights. However, the authors must acknowledge that one of the largest assumptions made in this analysis is that both the air and water inflatables could be filled to a sufficient pressure that their idealized shapes would remain fixed. Such an assumption allows for the use of rigid-body hydrodynamics calculated from WAMIT rather than attempting to model the flexibility of the inflatables [19]. Yet as discussed in the introduction, there are several research organizations that are exploring inflatable WEC designs that could lead to novel systems that can maintain unique shapes under the hydrostatic and dynamic pressures experienced when working in the wave environment. The next steps in the development of this two-body VGWEC concept will be to validate the numerical simulations against experimental data gath-

ered during a wave tank testing campaign in 2023. The results of the experimental campaign will first validate if the changes in geometry lead to the anticipated reductions in motion and corresponding loads. If successful, a follow-on series of experimental tests can be planned while attempting to include small-scale inflatables to better represent the true design.

ACKNOWLEDGMENTS

This work was authored in part by the National Renewable Energy Laboratory, operated by Alliance for Sustainable Energy, LLC, for the U.S. Department of Energy (DOE) under Contract No. DE-AC36-08GO28308. Funding provided by the U.S. Department of Energy Office of Energy Efficiency and Renewable Energy Water Power Technologies Office. The views expressed in the article do not necessarily represent the views of the DOE or the U.S. Government. The U.S. Government retains and the publisher, by accepting the article for publication, acknowledges that the U.S. Government retains a nonexclusive, paid-up, irrevocable, worldwide license to publish or reproduce the published form of this work, or allow others to do so, for U.S. Government purposes.

REFERENCES

[1] Tom, Nathan, Yu, Yi-Hsiang, Wright, Alan and Lawson, Michael. "Development of a nearshore oscillating surge wave energy converter with variable geometry." *Renewable Energy* Vol. 96 (2016): pp. 410–424. DOI http://dx.doi.org/10.1016/j.renene.2016.04.016.

[2] Husain, Salman, Davis, Jacob, Tom, Nathan, Thiagarajan, Krish, Burge, Cole and Nguyen, Nhu. "Influence on Structural Loading of a Wave Energy Converter by Controlling Variable-Geometry Components and the Power Take-Off." Vol. Volume 8: Ocean Renewable Energy. 2022. DOI 10.1115/OMAE2022-81518. URL https://doi.org/10.1115/OMAE2022-81518. _eprint: https://asmedigitalcollection.asme.org/OMAE/proceedings-pdf/OMAE2022/85932/V008T09A087/6929690/v008t09a087-omae2022-81518.pdf.

[3] Pecher, A. and Kofoed, J.P. and Larsen, T. and Marchalot, T. "Experimental study of the WEPTOS wave energy converter." *Proceedings of the 31st International Conference on Ocean, Offshore, and Arctic Engineering*. 2012. OMAE, Halifax, Canada.

[4] CalWave. "The xWave Series." Accessed 2023-1-09, URL https://calwave.energy/solutions/xwave/.

[5] Hamilton, Andrew, Cazenave, Francois, Forbush, Dominic, Coe, Ryan and Bacelli, Giorgio. "The MBARI-WEC: a power source for ocean sensing." *Journal of Ocean Engineering and Marine Energy* .

[6] Ogden, D., Tom, N., Van Rij, J., Guo, Y. and Yi-Hsiang, Y. "Numerical Modelling of a Two Body Point Absorber Featuring Variable Geometry." *Proceedings of the 14th European Wave and Tidal Energy Conference*. 2021. Plymouth, United Kingdom.

[7] Quocent. "Marine automatically stowable & inflatable volume (MASIV)." Technical Report No. Wave Energy Scotland Novel Wave Energy Converter Stage 1 Project Public Report NW11 _QUO_WEC PublicReport. 2017.

[8] Pardonner, Davy, Tom, Nathan and Guo, Y. "Numerical model development of a variable-geometry attenuator wave energy converter." *Proceedings of the 39th International Conference on Ocean, Offshore, and Arctic Engineering*. 2020.

[9] Greaves, D., Hann, M., Kurniwan, A., Chaplin, J. and Farley, F. "The hydrodynamics of air-filled bags for wave energy conversion." *Proceedings of the International Conference on Offshore Renewable Energy*. 2016. IEEE, Glasgow, Scotland.

[10] Driscoll, Frederick R., Weber, Jochem W., Jenne, Dale S., Thresher, Robert W., Fingersh, Lee J., Bull, Dianna, Dallman, Ann, Gunawan, Budi, Ruehl, Kelley, Newborn, David, Quintero, Miguel, LaBonte, Alison, Karwat, Darshan and Beatty, Scott. "Methodology to Calculate the ACE and HPQ Metrics Used in the Wave Energy Prize." Technical Report No. NREL/TP–5000-70592, 1426063. National Renewable Energy Laboratory. 2018. DOI 10.2172/1426063.

[11] Tom, Nathan, Yu, Yi-Hsiang and Wright, Alan. "Submerged pressure differential plate wave energy converter with variable geometry." *Proceedings of the 11th European Wave and Tidal Energy Conference*. 2019.

[12] Rosenberg, Brian J and Mundon, Timothy R. "Numerical and physical modeling of a flexibly-connected two-body wave energy converter." *Proceedings of the 4th Marine Energy Technology Symposium*: pp. 5–8. 2016. Washington DC, USA.

[13] Pizer, D. "Numerical Modelling of Wave Energy Absorbers." *Wave Project Report* .

[14] Salter, S.H. "Progress on Edinburgh ducks." *Proceedings of the IUTAM Symposium on Hydrodynamics of Ocean Wave Energy Utilization*: pp. 5–8. 1985. Lisbon, Portugal.

[15] "Rhinoceros 3D." Accessed 2023-1-9, URL https://www.rhino3d.com/.

[16] Lee, Chang Ho and Newman, John Nicholas. "Wamit user manual." *WAMIT, Inc* (2006): p. 42.

[17] Yu, Yi-Hsiang, Ruehl, Kelly, Van Rij, Jennifer, Tom, Nathan, Forbush, Dominic and Ogden, David. "WEC-Sim (Wave Energy Converter SIMulator) — WEC-Sim documentation." Accessed 2020-12-10, URL https:

//wec-sim.github.io/WEC-Sim/.

[18] Tom, Nathan, Yu, Yi-Hsiang, Wright, Alan and Lawson, Michael. "Balancing power absorption against structural loads with visouc drag and power-takeoff efficiency considerations." *IEEE Journal of Oceanic Engineering* Vol. 43 No. 4 (2018): pp. 1048–1067. DOI https://doi.org/10.1016/j.oceaneng.2019.04.063.

[19] Guo, Yi, Yu, Yi-Hsiang, van Rij, Jennifer and Tom, Nathan. "Inclusion of Structural Flexibility in Design Load Analysis for Wave Energy Converters." *12th European Wave and Tidal Energy Conference* (2017): pp. 1–6.